CrossMark

ORIGINAL PAPER

Sacrificial-Template-Assisted Syntheses of Aluminate and Titanate Nanonets via Interfacial Reaction Growth

Jian Shang[1] · Jiefeng Yu[1] · Yu Wang[2] ·
Majiong Jiang[1] · Yining Huang[1] · Donghan Yang[1] ·
Xin Tang[1] · Cong Gao[1] · Jianlong Li[1] ·
Wei Chen[3,4] · Guoqin Xu[3,4] · Boon K. Teo[1,5] ·
Kai Wu[1,4]

Abstract Crystalline $FeAlO_3$/$FeAl_2O_4$ nanonets were synthesized by a modified template-assisted approach using anodic aluminum oxide (AAO) as a reactive and sacrificial template to direct and promote interfacial reaction growth (IRG). The as-prepared nanonets replicate the morphology of the porous AAO template and contain mixed $FeAlO_3$ and $FeAl_2O_4$. To extend the applicability of the sacrificial-template-assisted IRG approach, porous anodic titanium oxide (ATO) was used as template in place of AAO, giving rise to Zn_2TiO_4 nanonet/nanotube and $PbTiO_3$ nanonet/nanotube. These latter products are polycrystalline due to the polycrystalline nature of the ATO template. Growth mechanism for the formation of the Zn_2TiO_4 and $PbTiO_3$ nanostructures is proposed. The present study shows that the IRG approach can be extended to fabricate patterned complex oxide nanomaterials that may find applications in a wide range of nanotechnologies such as electronics, photonics and spintronics.

✉ Boon K. Teo
boonkteo@gmail.com

✉ Kai Wu
kaiwu@pku.edu.cn

1 SKLSCUSS, BNLMS, College of Chemistry and Molecular Engineering, Peking University, Beijing 100871, China

2 School of Chemistry and Chemical Engineering, Chongqing University, Chongqing 400044, China

3 Department of Chemistry, National University of Singapore, Singapore 117543, Singapore

4 SPURc, 1 CREATE Way, #15-01, CREATE Tower, Singapore 138602, Singapore

5 Department of Chemistry, University of Illinois at Chicago, Chicago, IL 60607, USA

Introduction

Template-assisted synthesis, pioneered by Martin et al. in the late 1980s and early 1990s [1–4], has been one of the most popular methods for the fabrication of organic and inorganic nanomaterials. Template-assisted method can be integrated with various conventional approaches such as electrodeposition [4, 5], chemical vapor deposition [6], liquid phase reaction [7, 8], sol–gel method [9], hydrothermal method [10, 11], solvothermal method [12, 13], etc. In recent years, a variety of templates have been developed, including the so-called 'hard templates' exemplified by anodic aluminum oxide (AAO) (also known as porous anodic alumina, PAA), anodic titanium oxide (ATO), and track-etch polymeric membranes, as well as the so-called 'soft templates' such as micelle, DNA, protein, etc.

Among the typical hard templates, AAO attracts much attention due to its desirable attributes such as tunability of the porous structure, ease of preparation and temperature resistance. Traditionally, nanochannels in the AAO template are utilized as vessels to spatially guide the formation of well-oriented and patternable one-dimensional (1D) nanostructures such as nanowires, nanotubes, etc. The products usually replicate the uniformity and regularity of the AAO template, exhibiting a narrow distribution of the pore sizes. In this way, such a highly ordered nanocellular template is simply regarded as a physical scaffold which is eventually and selectively removed to yield 1D or two-dimensional (2D) arrays of nanostructures.

In recent years, an interfacial reaction growth (IRG) technique has been developed, utilizing either 1D or 2D nanostructures as the reactive and/or sacrificial template, in the fabrication of a wide variety of nanonet or nanotube array structures [14]. For example, Pt@$CoAl_2O_4$ peapods nanostructure [15] and $PbTiO_3$ nanocellular [16] had been prepared using 2D templates like AAO and ATO, while $ZnAl_2O_4$ nanotube [17, 18] and $MgAl_2O_4$ nanotube [19] were prepared on 1D templates. In a typical IRG approach, interfacial reaction(s) take place at the template surface when the incoming precursor (in either vapor, liquid or solid phase) encounters the surface. By employing laboratory-prepared AAO as the reactive template and metal oxide as the precursor in a reducing atmosphere, such an interfacial reaction leads to the formation of a layer of aluminate nanonet, which may be the target product or a buffer layer for further growth of metal oxide or metallic nanonets. The as-prepared nanomaterials closely replicate the morphology of the AAO template, forming arrays of nanonet [20–22] or nanotube/nanonet [23] structures.

Thus, a series of functional ternary oxide nanomaterials can be designed and tailor-made via the IRG technique. In this paper, we report the fabrication of 2D arrays of mixed ferric/ferrous aluminate ($FeAlO_3/FeAl_2O_4$) nanonets using AAO, and zinc titanate (Zn_2TiO_4) and lead titanate ($PbTiO_3$) nanotubes/nanonets using ATO, as reactive/sacrificial templates via the IRG method. It is known that $FeAlO_3$

is a piezoelectric, magnetoelectric and ferrimagnetic material, and polycrystalline $FeAlO_3$ had been shown to exhibit extremely high magnetic anisotropy at a temperature as low as 4.2 K [24]. To extend the applicability of the IRG approach and to broaden the nanomaterials base, we have explored another 2D template, namely, ATO nanotube array, and successfully prepared Zn_2TiO_4 nanotube/nanonet and $PbTiO_3$ nanotube/nanonet structures. Zn_2TiO_4 is a wide band-gap semiconductor with inverse spinel structure, and may have potential applications in photoelectrochemical and photoluminescent devices [25–27], or as a promising regenerable absorbent for removing H_2S from coal gasifier gas [27, 28]. $PbTiO_3$ belongs to a class of ABO_3-type perovskite materials, together with $PbZr_xTi_{1-x}O_3$, $BaTiO_3$, $SrTiO_3$, $Ba_xSr_{1-x}TiO_3$, etc. This group of functional materials exhibits excellent ferroelectric properties due to a high spontaneous polarization state which may find applications in micro-/nano-electronics [16, 29, 30]. It is hoped that the IRG approach described herein will pave the way for engineering and tailoring patternable functional ternary oxide nanomaterials.

Experimental Section

Preparation of AAO

Pure Al foil, pre-cleaned by 5 % NaOH solution to dissolve the topmost oxidized layer, was immersed in a mixed solution of ethanol and $HClO_4$ [4:1 (v/v)] at 0 °C and polished at 20 V with a Pt foil as the cathode. After the electropolishing process, the Al foil was rinsed by deionized water and then fixed in a home-made electrochemical cell as the anode. A solution of 0.3 M oxalic acid was employed as the electrolyte and the applied voltage was optimized to 40 V. The anodization process was ≤20 h. Afterwards, the AAO membrane was peeled off by an acid solution of 0.1 M $CuCl_2$ and 20 % HCl. To obtain membrane with both ends open, the capped barrier layer was further removed by 5 % H_3PO_4.

Preparation of $FeAlO_3/FeAl_2O_4$ Nanonets

As-prepared AAO template was immersed in a Fe_2O_3 (1 g)–ethanol (5 g) slurry and sonicated for 5 ∼ 10 min before being placed in a Muffle furnace. The furnace was heated to, and maintained at, 700 °C for 10 h before it was cooled to room temperature (RT). The as-treated AAO membrane was then buried in fresh Fe_2O_3 powders in a quartz boat. The boat was loaded into the flat temperature zone of a CVD device, which was then raised to 760 °C at the rate of 10 °C min^{-1}, with a high purity N_2 flow of 30 sccm at 1 atm. When the temperature reached the set-point, the gas flow was switched to H_2 with a flow rate of 30 sccm. The sample was kept in the CVD device for a certain period of time (300–2000 min) while maintaining the H_2 flow. Finally the CVD device was allowed to cool to RT in an N_2 flow.

Preparation of Zn_2TiO_4 Nanonet/Nanotube and $PbTiO_3$ Nanonet/Nanotube

ATO template was prepared by anodization of Ti foil (99.7 %, 0.25 mm) in a fluoride-containing electrolyte (0.3 wt% NH_4F+1 wt% H_2O in ethylene glycol). Prior to anodization, Ti foil (3.5×4 cm^2) was ultrasonically cleaned in acetone, ethanol, deionized (DI) water, and then dried at RT. Anodization was performed in a two-electrode device. The applied voltage was set at 60 V. After 24–48 h of anodization, the substrate, on which ATO membrane was firmly attached, was rinsed with ethanol and annealed at 340 °C for 60–120 min. After the annealing process, the sample was rinsed in ethanol again and sonicated to completely remove the debris piled on the obverse side of ATO membrane. In order to fabricate freestanding TiO_2 nanotube arrays with both ends open (as in the case of AAO), a secondary anodization was carried out in the same stock electrolyte at 12 V for 5–10 h. The sample was then immersed in 10 % H_2O_2 for 12–24 h during which the ATO membrane peeled off spontaneously. The free-standing membrane was further treated with HF vapor for several hours to remove the barrier layer which capped the bottom of the TiO_2 nanotubes (via erosion).

To prepare the Zn_2TiO_4 nanonet/nanotube, the as-prepared TiO_2 membrane was immersed in a slurry of (high-purity, 1 g) ZnO in ethanol (5 g) in a crucible. After sonicated for several minutes, the crucible was placed in a Muffle furnace and kept at 500 °C for 3 h. The as-treated ATO membrane was then planted in fresh ZnO powders in a quartz boat, and placed in a CVD device. The temperature of the furnace was raised to 600 °C in 60 min in an N_2 flow of 30 sccm (at a pressure of 1 atm). Gas flow was switched over to H_2 (1 atm) at the rate of 30 sccm and the sample was kept at 600 °C for a certain period of time (200–1000 min). Finally it was cooled to RT in an N_2 flow.

Similarly, to prepare the $PbTiO_3$ nanonet/nanotube, the as-prepared ATO template was then immersed in a slurry of PbO_2 (1 g) in ethanol (5 g) in a crucible. After sonicated for about 10 min, the crucible was placed into a Muffle furnace. The furnace was kept at 500–600 °C for 24–48 h, and then cooled to RT.

Characterization

To prepare samples for transmission electron microscope (TEM) and high-resolution TEM (HRTEM) examinations, the as-prepared $FeAlO_3$/$FeAl_2O_4$ nanonets were dispersed in 40 % (wt) HF solution, whereas the Zn_2TiO_4 and $PbTiO_3$ nanonet samples were obtained by ion-milling.

Characterization and analysis were carried out on scanning electron microscope (SEM, Hitachi S4800), environmental SEM (ESEM, Quanta 200F, FEI), TEM (JEM 200CX JEOL), HRTEM (Tecnai F30 & F20, Philips), X-ray diffraction (XRD, Rigaku D/MAX-200 X-ray powder diffractometer) in which a Cu K_α ($\lambda = 0.154$ nm) radiation source was used, and X-ray photoelectron spectroscopy (XPS, Kratos Axis Ultra spectrometer), in which a monochromated Al K_α (1486.6 eV) radiation source of 225 W (15 mA, 15 kV) in power output was employed and the binding energies were calibrated with hydrocarbon C 1 s peak at 284.8 eV.

Results and Discussions

FeAlO$_3$/FeAl$_2$O$_4$ Nanonet

FeAlO$_3$/FeAl$_2$O$_4$ nanonets were obtained at 760–780 °C via the IRG method using AAO template. It can be seen from the SEM images (Figs. 1a, b) that the highly ordered morphology of the AAO template was largely retained. The TEM images, depicted in Figs. 1c, d, show highly ordered nanonet structures as large as tens of square microns.

Selected-area electron diffraction (SAED) patterns (insets in Figs. 2a, b) of the FeAlO$_3$/FeAl$_2$O$_4$ nanonets reveal that the nanonets comprise of highly crystalline FeAlO$_3$ (Fig. 2a) and FeAl$_2$O$_4$ (Fig. 2b). The corresponding HRTEM images are depicted in Fig. 2c, d for domains of FeAlO$_3$ and FeAl$_2$O$_4$ (with the *insets* being the respective simulated FFT patterns). The interplanar spacing of 0.338 nm and 0.361 nm (measured from Fig. 2c) correspond to the $(\bar{2}11)$ and (021) facets of FeAl$_2$O$_4$ (JCPDS 34-0192), while the interplanar distances of 0.337 nm, 0.342 nm, and 0.245 nm (measured from Fig. 2d) are in good agreement with the the $(02\bar{1})$, (021) and (002) facets of FeAlO$_3$ (JCPDS 30-0024). XPS spectra (Fig. S1, Supporting Information) also confirm the existence of both Fe(III) and Fe(II) in the nanonets. Thus, the nanonets can be characterized as admixtures of crystalline FeAlO$_3$ and FeAl$_2$O$_4$. However, it was difficult to determine the ratio of the two components owing to the interference caused by the large amount of δ-Al$_2$O$_3$ present in the as-prepared products.
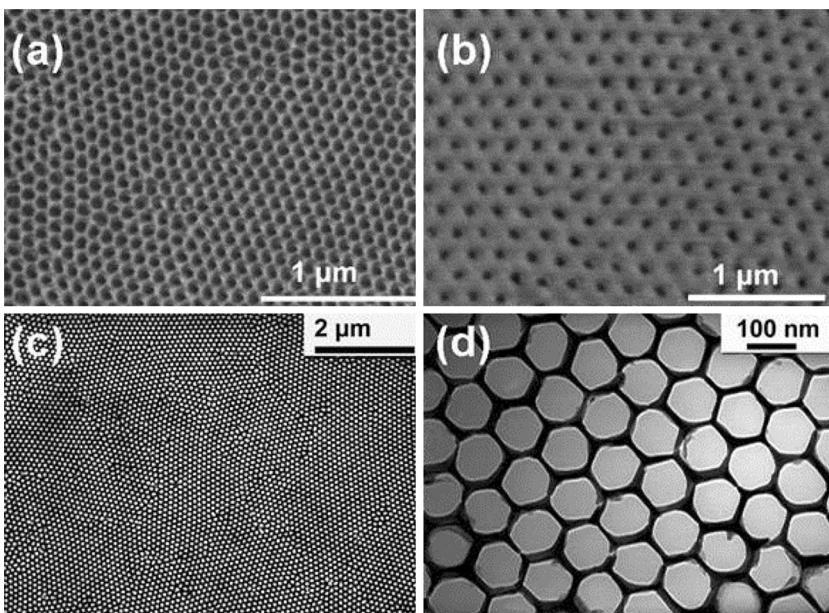
Fig. 1 SEM images of **a** *top side view* and **b** *bottom side view* of as-prepared FeAlO$_3$/FeAl$_2$O$_4$ nanonets. Large scale **c** and enlarged **d** TEM images of FeAlO$_3$/FeAl$_2$O$_4$ nanonets
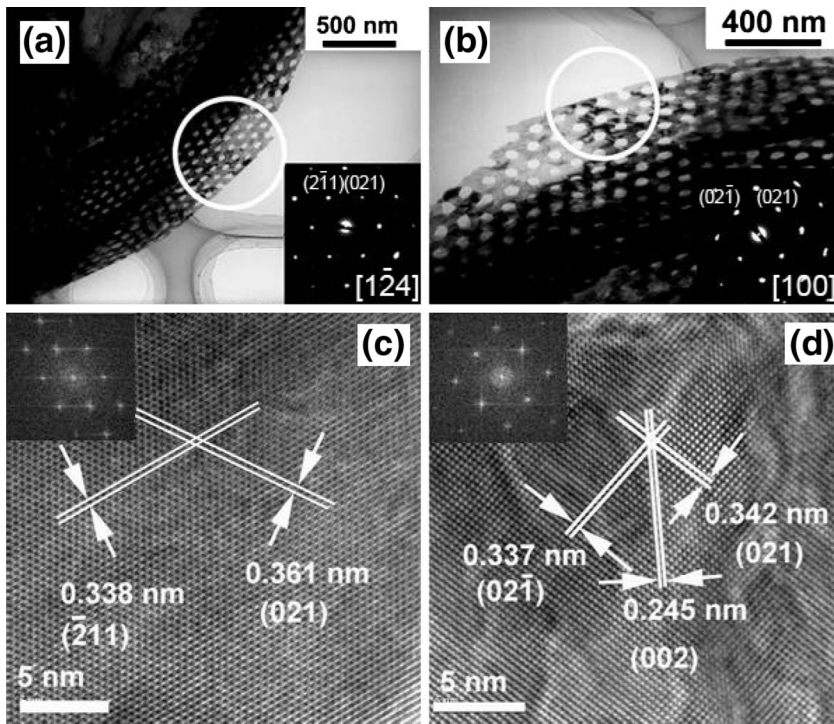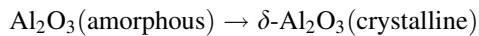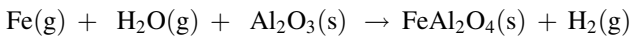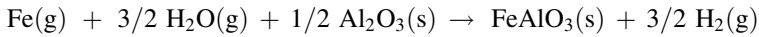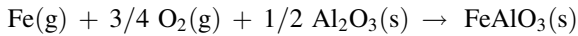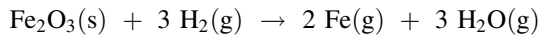
Fig. 2 SAED patterns (*insets* in **a** and **b**), recorded from the edges of FeAlO$_3$/FeAl$_2$O$_4$ nanonets (indicated by *circles*), reveal two kinds of crystal structures corresponding to FeAlO$_3$ (**a**) and FeAl$_2$O$_4$ (**b**). The corresponding HRTEM images are: **c** FeAlO$_3$ and **d** FeAl$_2$O$_4$ (the insets are the respective simulated FFT patterns)

However, we were unable to prepare pristine FeAlO$_3$ nanostructures since its stability range in the binary equilibrium diagram of Fe$_2$O$_3$–Al$_2$O$_3$ is rather narrow [31]. There were substantial efforts in the literature with regards to the preparation and characterization of pure FeAlO$_3$. Conventional syntheses of FeAlO$_3$ mainly include a simple solid-state reaction method [32–34], and a two-step approach of sintering the coprecipitation product of aluminum nitrate and iron nitrate by adding ammonium hydroxide solution [31]. Unconventional syntheses such as the decomposition of mixed oxalic salt like (NH$_4$)$_3$[Fe$_{0.50}$Al$_{0.50}$(C$_2$O$_4$)$_3$]·3H$_2$O, followed by an annealing process to yield FeAlO$_3$, have also been reported [24, 35]. Contrary to these approaches which generally employ extremely high temperatures over 1000 °C, our method requires a much milder condition (760 °C).

We propose the following mechanism for the IRG of FeAlO$_3$/FeAl$_2$O$_4$ nanonets using AAO as the reactive and sacrificial template. In the CVD furnace, iron vapor, generated by thermal reduction of Fe$_2$O$_3$ in the H$_2$ atmosphere, diffused to the surface of the AAO template. Interfacial reactions took place in the presence of residual O$_2$ and H$_2$O. This mechanism is similar to that proposed previously by us for the IRG growth of zinc aluminate [22, 23]. However, due to the multi-valence of

iron, incomplete oxidization of iron atoms resulted in the formation of the $FeAl_2O_4$. At the same time, amorphous AAO template partly transformed into δ-Al_2O_3 (Fig. S2). The proposed reactions are listed as follows:

$$Fe_2O_3(s) \; + \; 3 \; H_2(g) \; \rightarrow \; 2 \; Fe(g) \; + \; 3 \; H_2O(g)$$

$$Fe(g) \; + \; 3/4 \; O_2(g) \; + \; 1/2 \; Al_2O_3(s) \; \rightarrow \; FeAlO_3(s)$$

$$Fe(g) \; + \; 3/2 \; H_2O(g) \; + \; 1/2 \; Al_2O_3(s) \; \rightarrow \; FeAlO_3(s) \; + \; 3/2 \; H_2(g)$$

$$Fe(g) \; + \; 1/2 \; O_2(g) \; + \; Al_2O_3(s) \; \rightarrow \; FeAl_2O_4(s)$$

$$Fe(g) \; + \; H_2O(g) \; + \; Al_2O_3(s) \; \rightarrow \; FeAl_2O_4(s) \; + \; H_2(g)$$

$$Al_2O_3(amorphous) \rightarrow \delta\text{-}Al_2O_3(crystalline)$$

The vapor pressure of Fe at 760–780 °C is insufficient to maintain a sustainable vapor–solid (V–S) growth. There were reports [36, 37] of the growth of Fe_2O_3 nanowires or nanobelts by direct heating of a Fe foil in an oxidizing atmosphere like O_2 at 600–800 °C. Both authors ascribed the mechanism for the formation of such nanostructures to Fe atom diffusion or ion diffusion rather than vapor–liquid–solid (V–L–S) or V–S mechanism, citing low vapor pressure of Fe as the major reason (since the temperature employed was much lower than the melting point of Fe and Fe_2O_3). However, it has been reported that ionic compounds like oxides, could spontaneously form a monolayer at the surface of Al_2O_3 powder at a temperature much lower than their melting points [38, 39]. This spontaneous monolayer dispersion might be responsible for the formation of Mo and Cu nanonets as we have demonstrated [20], and could possibly promote the condensation and spreading of iron-containing species in the present case as well. The dispersion phenomenon could be crucial for the synthesis of nanomaterials, especially when a thermal pretreatment of the precursors was employed. Li et al. [40] claimed that a thermal treatment of Fe_2O_3 and Ga_2O_3 powder prior to reduction and nitridation will evidently induce the doping of Fe into GaN nanowires. Similarly, it is expected that the thermal pretreatment and the monolayer dispersion indeed can promote the interfacial reaction at the surface of AAO template, overcoming the unfavorable factor of low Fe vapor pressure.

As we have demonstrated, diffusion of the involved reactive species plays a key role in the IRG approach, which can affect the composition and morphology of the final products. In addition, crystalline nature of the AAO template could also have lowered its reactive activity. As a result of both factors, in the synthesis of $FeAlO_3$/$FeAl_2O_4$ nanonets, interfacial reaction just took place at the exterior surface of the AAO template, without involving the interior surface to yield nanotubes simultaneously as in the synthesis of zinc aluminate. After all, a diffusion-limited interfacial reaction finally resulted in the formation of the sheer $FeAlO_3$/$FeAl_2O_4$ nanonets, similar to the case of $Ga_2O \cdot 11Al_2O_3$ nanonet, also fabricated via IRG, reported previously by us [21].

Zn$_2$TiO$_4$ Nanonet/Nanotube

Preparation of the ATO template is similar to the method reported by Chen et al. [41] and Paulose et al. [42] Semi-transparent ATO membranes, as large as the original Ti foil (about 3.5 × 4 cm^2), were obtained (Fig. 3a). Due to the erosion of the F$^-$ ion during the electrochemical process, the obverse surface of the ATO membrane (Fig. 3b) is not as flat and regular as the AAO one, while the reverse side is relatively flat in large area except for the protuberant barrier layer which caps the nanotubes (Fig. 3c). As shown in Fig. 3d, open-ended ATO membrane, with domains as large as hundreds of micron squares of well-organized networks of nanopores, can be obtained by chemical etching treatment. Free-standing ATO membranes of such a structure are considered as an 'ideal' template for interfacial reaction growth, since unimpeded channels would be propitious for the transport of the precursor vapor, and the flat and ordered nanonet structure would improve the morphology of the products.
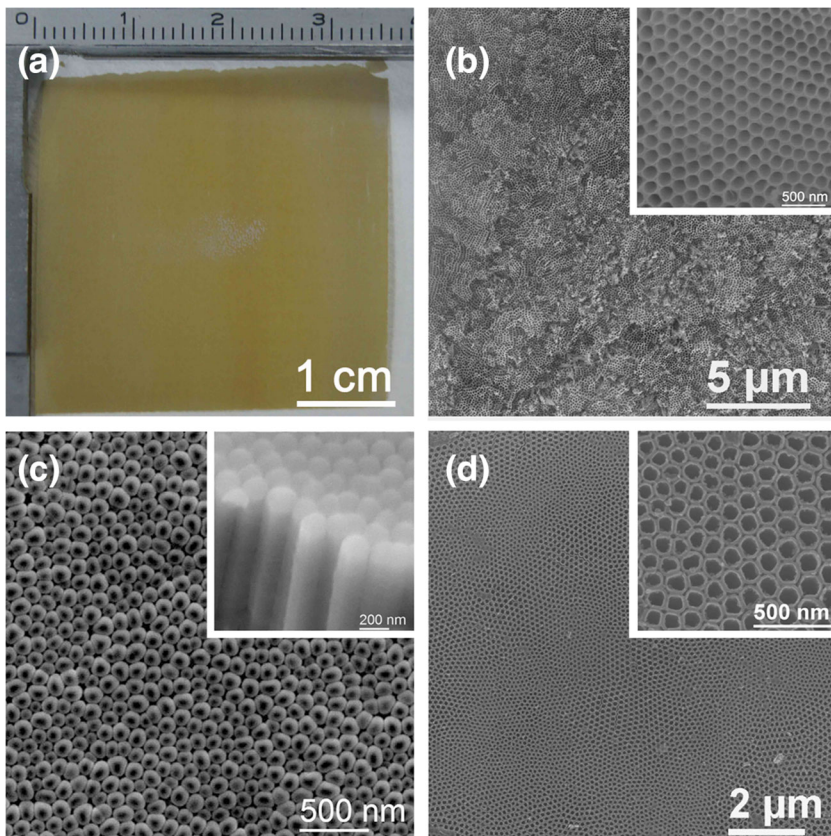
**Fig. 3** **a** Digital image of a sheet ATO membrane as large as 3.5 × 4 cm^2. SEM images of the obverse side **b** and reverse side **c** of ATO templates. **d** SEM image of the reverse side of an open-ended ATO template. (*Insets* are enlarged images.)

The SEM and TEM of the Zn_2TiO_4 nanonets/nanotubes are depicted in Figs. 4 and 5, respectively. The SEM images revealed a fusion tendency in the reaction of ZnO with TiO_2 and H_2, converting individual TiO_2 nanotubes of the template into a seamless Zn_2TiO_4 nanonets in the IRG growth, as shown in Figs. 4a–c. Furthermore, in the process of the transformation from the ATO template to the Zn_2TiO_4 nanostructures, nanonets were observed from both sides of the membrane. XRD data revealed the formation of Zn_2TiO_4 (JCPDS 86-0156). No diffraction peaks indicative of ZnO or TiO_2 (anatase) were observed. Thus it was concluded that the sacrificial ATO template was completely converted into Zn_2TiO_4 via interfacial reactions with the retention of the morphology of the template.

Also observed were Zn_2TiO_4 nanotubes under TEM examination. A typical Zn_2TiO_4 nanotube is portrayed in Fig. 5a. HRTEM characterization displays an interplanar distance of 0.354 nm (cf. Fig. 5b), corresponding to the (210) diffraction planes of Zn_2TiO_4 (JCPDS 86-0156). Well-organized Zn_2TiO_4 nanonet is shown in Fig. 5c, and the interplanar distance of 0.355 nm, 0.357 nm fits well with (210) and
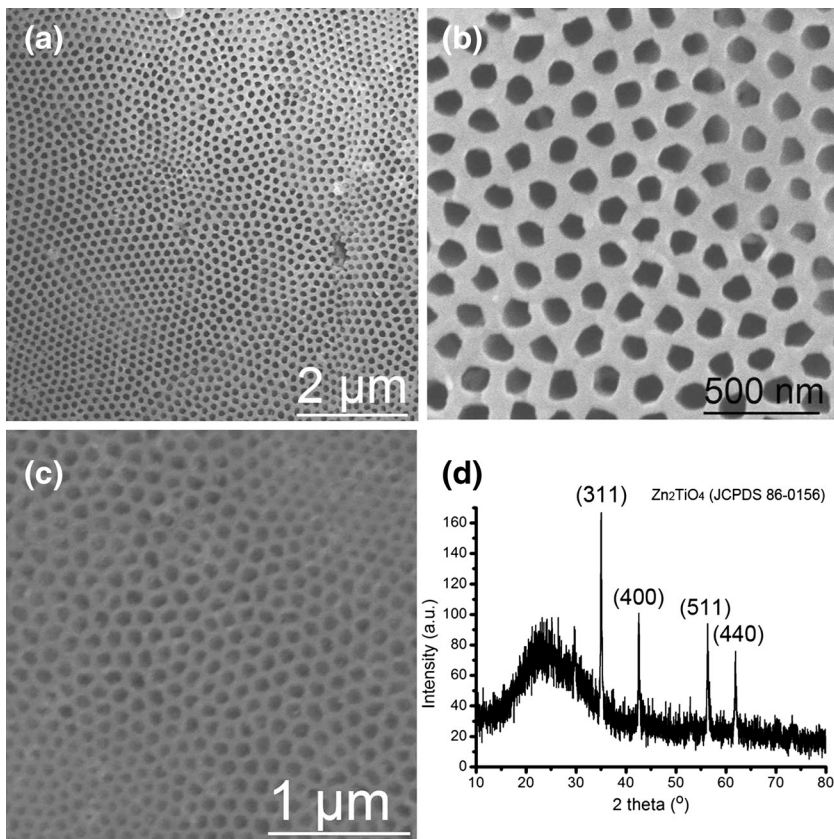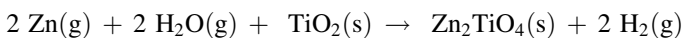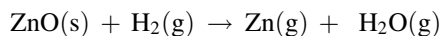

Fig. 4 **a** SEM images of the obverse side of Zn_2TiO_4 nanonet. **b** A higher magnification of (**a**). **c** SEM image of the reverse side of Zn_2TiO_4 nanonet. **d** XRD spectrum of the prepared sample, showing the sharp diffraction features of Zn_2TiO_4 (JCPDS 86-0156)
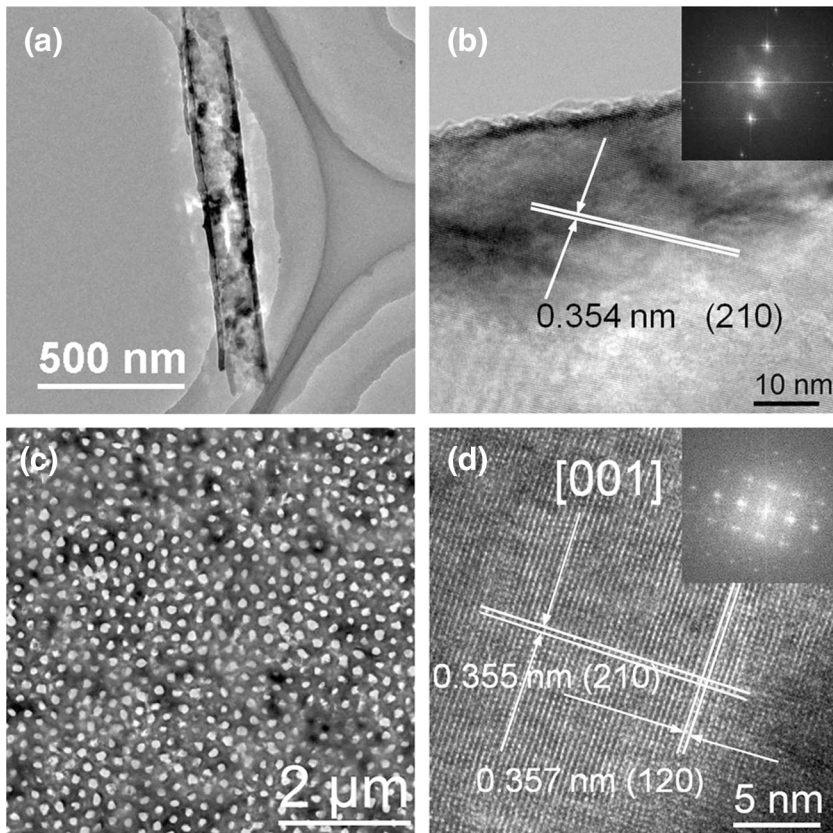
Fig. 5 TEM image (**a**) and HRTEM image (**b**) of a Zn_2TiO_4 nanotube. TEM image (**c**) and HRTEM image (**d**) of a Zn_2TiO_4 nanonet. (*Insets* of **b** and **d** are the corresponding simulated FFT patterns)

$(1\bar{2}0)$ facets of Zn_2TiO_4 (Fig. 5d), respectively. In addition, we also examined different sites of the Zn_2TiO_4 nanonets, and found that they were predominantly polycrystalline in nature (Fig. S3).

Similar to the IRG of $ZnAl_2O_4$ nanonet, mechanism for the formation of Zn_2TiO_4 nanonet may be described as follows:

$$ZnO(s) + H_2(g) \rightarrow Zn(g) + H_2O(g)$$

$$2\,Zn(g) + 2\,H_2O(g) + TiO_2(s) \rightarrow Zn_2TiO_4(s) + 2\,H_2(g)$$

$$2\,Zn(g) + O_2(g) + TiO_2(s) \rightarrow Zn_2TiO_4(s)$$

We note that Yi et al. [43] and Yang et al. [44] reported the fabrication of Zn_2TiO_4 nanowires by employing ZnO nanowires as templates. Core–shell ZnO/Ti and ZnO/TiO_2 nanostructures were annealed to produce Zn_2TiO_4 nanowires. Unlike previous reports on the preparation of $ZnAl_2O_4$ [17, 18] and $MgAl_2O_4$ [19] via the same strategy, both authors claimed that no nanotube and void (which indicated the

Kirkendall effect) was observed in the as-prepared Zn_2TiO_4 nanowires, and attributed the phenomenon to a faster diffusion rate of Ti^{4+} than that of Zn^{2+} [43–45]. Besides, Cheng et al. [46] fabricated Zn_2TiO_4–ZnO nanowires via similar approach, and proposed a Zn^{2+} unilateral diffusion mechanism rather than counter diffusion for the formation of the as-prepared axial heterostructures. In fact, as-mentioned synthetic strategy, in which a solid–solid reaction was utilized, could be ascribed to IRG approach as well. To illustrate the mechanism of our synthesis, we conducted a control experiment in which N_2 was introduced into the quartz tube instead of H_2 and no formation of Zn_2TiO_4 could be identified. This result indicated that the relative lower temperature employed here could not trigger the solid-state reaction, and confirmed the IRG mechanism triggered by Zn atom diffusion as proposed above.

In a previous work, we demonstrated that IRG could take place at both the interior and exterior surfaces of an AAO template, resulting in a nanotube/nanonet structure [23]. In the case of the ATO template, its fused nanotube structure implies the potential of triggering the interfacial reaction at both the interior and exterior surfaces of TiO_2 nanotubes. In other words, considering the nanotube arrays of the ATO template rather than the nanocellular structure of AAO, the exterior surface of the nanotube could also be involved. Thus, synthesis of Zn_2TiO_4 nanonets involves the diffusion of zinc vapor into the TiO_2 nanotubes as well as the space between the tubes, resulting in gas–solid interfacial reaction and deposition of Zn_2TiO_4 on both the inner and the outer surfaces of the nanotubes. As the formation of Zn_2TiO_4 continues, the nanotube walls thicken, leading to a smaller tube diameter, and eventually giving rise to a seamless nanonet or so-called nanocellular structure with the voids between the tubes being completely filled. The net result is a volume expansion as revealed by the SEM images (cf. Fig. 4). We note that the strategy of utilizing the exterior surfaces of the ATO tube walls in a templated growth of nanomaterials is not new. Schmuki and co-workers [47] reported selective filling of the interspace with polypyrrole by electropolymerization, thus realizing one-step fabrication of nanopore arrays (or so-called nanocellular structure) by employing the exterior tube walls as the template, instead of the conventional two-step replication strategy.

As for the polycrystalline nature of the Zn_2TiO_4 nanostructures, it is proposed that the ATO template, initially amorphous in nature, had become polycrystalline anatase (JCPDS 21-1272) at 400 °C (Fig. S4). The sacrificial polycrystalline template then gave rise to the polycrystalline Zn_2TiO_4 product via the IRG at 600 °C.

$PbTiO_3$ Nanonet/Nanotube

Conventional syntheses of perovskite ABO_3-type nanomaterials include mainly electrodeposition [48], sol–gel [49], solid–solid reactions [50, 51], and so on and so forth, either with or without AAO templates. In recent years, with the emerging of TiO_2 nanotube array prepared by a simple electrochemical process, similar $PbTiO_3$ nanostructures were fabricated by different routes [16, 52], and its PL spectrum [53], Curie temperature [54] as well as piezoelectric hysteresis loop [16] were investigated. In analogy to the synthesis of the Zn_2TiO_4 nanostructures, we have
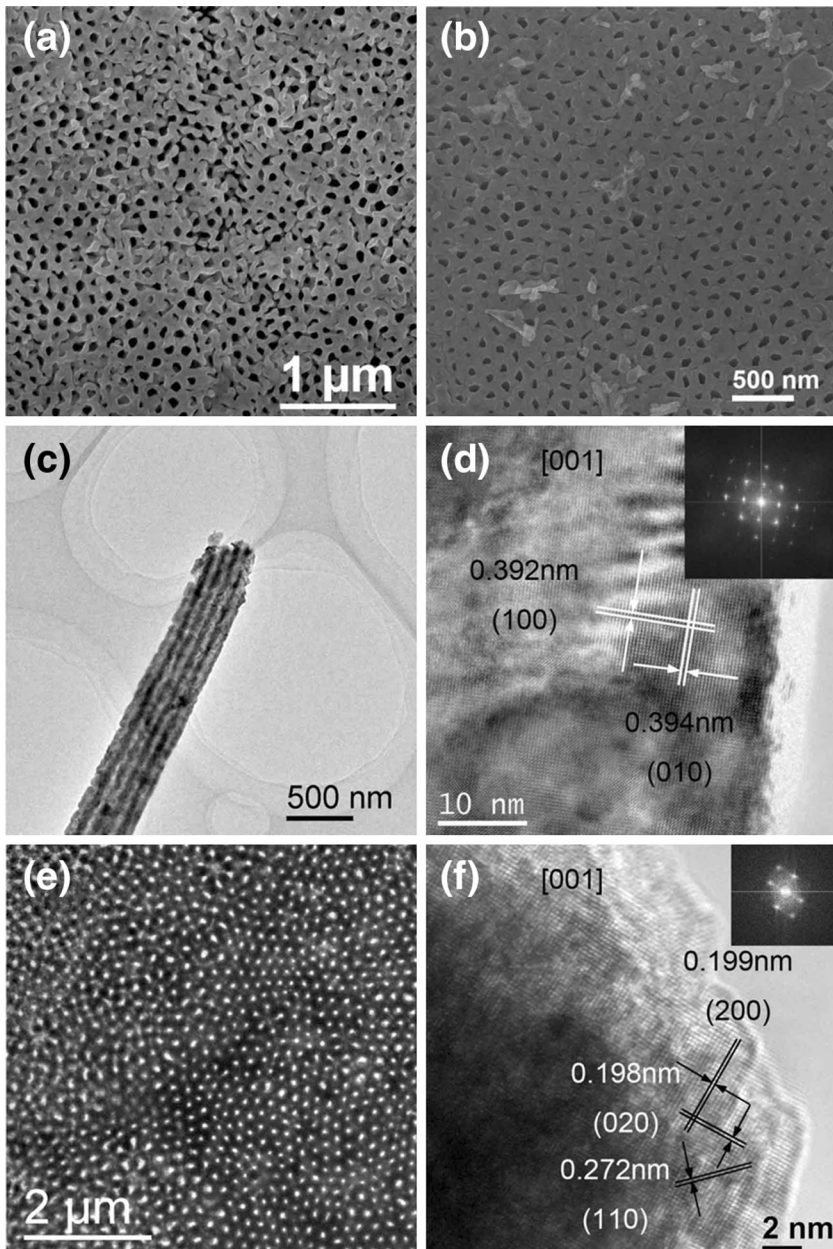
Fig. 6 SEM images of the obverse side **a** and reverse side **b** of as-prepared PbTiO$_3$ nanonet. TEM image **c** and HRTEM image **d** of a PbTiO$_3$ nanotube. TEM image **e** and HRTEM image **f** of a PbTiO$_3$ nanonet. (*Insets* of **d** and **f** are the corresponding simulated FFT patterns.)

also prepared $PbTiO_3$ nanonet/nanotube via the IRG method involving a solid–solid interfacial reaction.

The mechanism for this process is explicit, for a solid–solid reaction takes place at the exterior surface of the ATO template and reactive species incessantly diffuse into the template with a volume expansion:

$$TiO_2(s) + PbO(s) \rightarrow PbTiO_3(s)$$
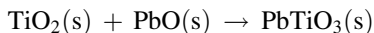
Thus, the ATO template was converted into $PbTiO_3$ nanonet/nanotube, or so-called nanocellular structures. Temperature is a key parameter in controlling this conversion and the morphology of the resulted products (Fig. S5). Fig. 6a, b depict the obverse and the reverse sides, respectively, of the $PbTiO_3$ nanostructures prepared under the optimized conditions. It is clear that the reverse side appears as a well-organized nanonet with relatively flat areas. Representative TEM and HRTEM images of the $PbTiO_3$ nanotubes are shown in Figs. 6c, d. The interplanar spacing of the tube wall is measured to be 0.392 nm and 0.394 nm, matching with (100) and (010) lattice planes of tetragonal $PbTiO_3$ (JCPDS 06-0452). TEM image of the $PbTiO_3$ nanonet is given in Fig. 6e, and the interplanar distances of 0.199 and 0.198 nm corresponds to (200) and (020) facets of $PbTiO_3$ (Fig. 6f). As revealed by the HRTEM images, the as-prepared $PbTiO_3$ nanonet/nanotube is polycrystalline, just as in the case of Zn_2TiO_4.

Conclusion

In summary, $FeAlO_3/FeAl_2O_4$ nanonets were prepared via a modified CVD approach, namely, interfacial reaction growth (IRG) using AAO as a reactive and sacrificial template. By replacing AAO with ATO, we succeeded in the preparation of Zn_2TiO_4 and $PbTiO_3$ nanonets/nanotubes. The mechanism for the formation of $FeAlO_3/FeAl_2O_4$ and Zn_2TiO_4 nanostructures mainly includes a thermal reduction of the precursors and an interfacial reaction involving the templates, similar to that proposed previously by us for the preparation of the $ZnAl_2O_4$ nanostructures. As for $PbTiO_3$, a simple solid–solid interfacial reaction was utilized, converting the ATO template to $PbTiO_3$ nanostructures. Different from the IRG with AAO, all the products derived from ATO template were polycrystalline due to the polycrystalline nature of the template itself. It is taken that IRG is an efficient strategy towards various kinds of materials and nanostructures, especially for 2D functional complex oxide nanomaterials.

To expand the applicability of the IRG approach and to prepare different classes of functional nanomaterials such as niobate and the likes, it is important to develop novel templates. Valve metals such as Al, Ti and Nb [55], Zr [56], Ta [57] and W [58] as well can form a compact oxide layer with desirable nanostructures through electrochemical anodization. These nanostructures can serve as reactive and/or sacrificial templates. Besides, zero-dimensional (0D) and 1D nanomaterials can also serve as secondary templates in the fabrication of either porous or solid nanostructures via the IRG strategy. Finally, the IRG approach has the natural advantage of forming core–shell structures. By making use of patternable reactive and/or sacrificial templates coupled with different types of solid–solid, solid–liquid and vapor–solid interfacial reactions,

the range of the IRG approach can be greatly extended in the engineering and tailoring of a wide variety of functional nanomaterials.

Author Contribution   The manuscript was written through contributions of all authors, and all authors have given approval to the final version of the manuscript.

References

1. Z. Cai and C. R. Martin (1989). *J. Am. Chem. Soc.* **111**, 4138–4139.
2. C. R. Martin, L. S. Van Dyke, Z. Cai, and W. Liang (1990). *J. Am. Chem. Soc.* **112**, 8976–8977.
3. C. J. Brumlik and C. R. Martin (1991). *J. am. chem. soc.* **113**, 3174–3175.
4. C. R. Martin (1994). *Science* **266**, 1961–1966.
5. X. J. Wu, F. Zhu, C. Mu, Y. Liang, L. Xu, Q. Chen, R. Chen, and D. Xu (2010). *Coord. Chem. Rev.* **254**, 1135–1150.
6. X. P. Shen, H. J. Liu, X. Fan, Y. Jiang, J. M. Hong, and Z. Xu (2005). *J. Cryst. Growth* **276**, 471–477.
7. Y. Mao and S. S. Wong (2004). *J. Am. Chem. Soc.* **126**, 15245–15252.
8. F. Zhang and S. S. Wong (2009). *Chem. Mater.* **21**, 4541–4554.
9. B. Cheng and E. T. Samulski (2001). *J. Mater. Chem.* **11**, 2901–2902.
10. J. Wan, X. Chen, Z. Wang, X. Yang, and Y. Qian (2005). *J. Cryst. Growth* **276**, 571–576.
11. X. Zhu, J. Ma, Y. Wang, J. Tao, J. Zhou, Z. Zhao, L. Xie, and H. Tian (2006). *Mater. Res. Bull.* **41**, 1584–1588.
12. T. Thongtem, A. Phuruangrat, and S. Thongtem (2009). *Cryst. Res. Technol.* **44**, 865–869.
13. H. Su, Y. Xie, P. Gao, H. Lu, Y. Xiong, and Y. Qian (2000). *Chem. Lett.* **29**, 790–791.
14. J. Yu, F. Wang, Y. Wang, H. Gao, J. Li, and K. Wu (2010). *Chem. Soc. Rev.* **39**, 1513–1525.
15. L. Liu, W. Lee, R. Scholz, E. Pippel, and U. Gösele (2008). *Angew. Chem. Int. Ed.* **47**, 7004–7008.
16. J. M. Macak, C. Zollfrank, B. J. Rodriguez, H. Tsuchiya, M. Alexe, P. Greil, and P. Schmuki (2009). *Adv. Mater.* **21**, 3121–3125.
17. Y. Yang, D. S. Kim, M. Knez, R. Scholz, A. Berger, E. Pippel, D. Hesse, U. Gosele, and M. Zacharias (2008). *J. Phys. Chem. C* **112**, 4068–4074.
18. J. F. Hong, M. Knez, R. Scholz, K. Nielsch, E. Pippel, D. Hesse, M. Zacharias, and U. Gosele (2006). *Nat. Mater.* **5**, 627–631.
19. H. Fan, M. Knez, R. Scholz, K. Nielsch, E. Pippel, D. Hesse, U. Gosele, and M. Zacharias (2006). *Nanotechnology* **17**, 5157.
20. F. Wang, Y. Wang, J. Yu, Y. Xie, J. Li, and K. Wu (2008). *J. Phys. Chem. C* **112**, 13121–13125.
21. Y. Wang, W. Wen, and K. Wu (2010). *Sci. China Chem.* **53**, 438–444.
22. Y. Wang, Q. Liao, H. Lei, X. P. Zhang, X. C. Ai, J. P. Zhang, and K. Wu (2006). *Adv. Mater.* **18**, 943–947.
23. Y. Wang and K. Wu (2005). *J. Am. Chem. Soc.* **127**, 9686–9687.
24. F. Bouree, J. L. Baudour, E. Elbadraoui, J. Musso, C. Laurent, and A. Rousset (1996). *Acta Crystallogr Sect. B* **52**, 217–222.
25. S. A. Mayén-Hernández, G. Torres-Delgado, R. Castanedo-Pérez, J. Márquez-Marín, M. Gutiérrez-Villarreal, and O. Zelaya-Angel (2008). *Sol. Energy Mater. Sol. Cells* **91**, 1454–1457.
26. K. H. Yoon, J. Cho, and D. H. Kang (1999). *Mater. Res. Bull.* **34**, 1451–1461.
27. A. C. Chaves, S. J. G. Lima, R. C. M. U. Araújo, M. A. M. A. Maurera, E. Longo, P. S. Pizani, L. G. P. Simões, L. E. B. Soledade, A. G. Souza amd, and I. M. G. Santos (2006). *J. Solid State Chem.* **179**, 985–992.
28. K. Jothimurugesan and S. K. Gangwal (1998). *Ind. Eng. Chem. Res.* **37**, 1929–1933.
29. M. W. Chu, I. Szafraniak, R. Scholz, C. Harnagea, D. Hesse, M. Alexe, and U. Gosele (2004). *Nat. Mater.* **3**, 87–90.
30. I. Vrejoiu, M. Alexe, D. Hesse, and U. Gösele (2008). *Adv. Funct. Mater.* **18**, 3892–3906.

31. M. E. Villafuerte-Castrejón, E. Castillo-Pereyra, J. Tartaj, L. Fuentes, D. Bueno-Baqués, G. González, and J. A. Matutes-Aquino (2004). *J. Magn. Magn. Mater.* **272–276**, 837–839.
32. A. Muan and C. L. Gee (1956). *J. Am. Ceram. Soc.* **39**, 207–214.
33. L. M. Atlasamd and W. K. Sumida (1958). *J. Am. Ceram. Soc.* **41**, 150–160.
34. R. R. Dayal, J. A. Gard, and F. P. Glasser (1965). *Acta Crystallogr.* **18**, 574–575.
35. X. Devaux, A. Rousset, J. M. Broto, H. Rakoto, and S. Askenazy (1990). *J. Mater. Sci. Lett.* **9**, 371–372.
36. X. Wen, S. Wang, Y. Ding, Z. L. Wang, and S. Yang (2004). *J. Phys. Chem. B* **109**, 215–220.
37. Y. Y. Fu, R. M. Wang, J. Xu, J. Chen, Y. Yan, A. V. Narlikar, and H. Zhang (2003). *Chem. Phys. Lett.* **379**, 373–379.
38. Y. Xie, N. Yang, Y. Liu, and Y. Tang (1982). *Sci. China Ser. B* **8**, 673–682.
39. Y. C. Xie and Y. Q. Tang (1990). *Adv. Catal.* **37**, 1–43.
40. Y. Li, C. Cao, and Z. Chen (2010). *J. Phys. Chem. C* **114**, 21029–21034.
41. Q. Chen and D. Xu (2009). *J. Phys. Chem. C* **113**, 6310–6314.
42. M. Paulose, H. E. Prakasam, O. K. Varghese, L. Peng, K. C. Popat, G. K. Mor, T. A. Desai, and C. A. Grimes (2007). *J. Phys. Chem. C* **111**, 14992–14997.
43. Y. Yang, X. Sun, B. Tay, J. Wang, Z. Dong, and H. Fan (2007). *Adv. Mater.* **19**, 1839–1844.
44. Y. Yang, R. Scholz, H. J. Fan, D. Hesse, U. Gösele, and M. Zacharias (2009). *ACS Nano* **3**, 555–562.
45. S. K. Manik, P. Bose, and S. K. Pradhan (2003). *Mater. Chem. Phys.* **82**, 837–847.
46. C. Cheng, W. Li, T. L. Wong, K. M. Ho, K. K. Fung, and N. Wang (2011). *J. Phys. Chem. C* **115**, 78–82.
47. D. Kowalski and P. Schmuki (2010). *Chem. Commun.* **46**, 8585–8587.
48. A. Nourmohammadi, M. Bahrevar, S. Schulze, and M. Hietschold (2008). *J. Mater. Sci.* **43**, 4753–4759.
49. L. Liu, T. Ning, Y. Ren, Z. Sun, F. Wang, W. Zhou, S. Xie, L. Song, S. Luo, D. Liu, J. Shen, W. Ma, and Y. Zhou (2008). *Mater. Sci. Eng. B* **149**, 41–46.
50. M. Teresa-Buscaglia, C. Harnagea, M. Dapiaggi, V. Buscaglia, A. Pignolet, and P. Nanni (2009). *Chem. Mater.* **21**, 5058–5065.
51. Z. Deng, Y. Dai, W. Chen, and X. Pei (2010). *J. Phys. Chem. C* **114**, 1748–1751.
52. Y. Yang, X. Wang, C. Zhong, C. Sun, and L. Li (2008). *Appl. Phys. Lett.* **92**, 122907.
53. Y. Yang, X. H. Wang, C. K. Sun, and L. T. Li (2008). *J. Am. Ceram. Soc.* **91**, 3820–3822.
54. Y. Yang, X. H. Wang, C. K. Sun, and L. T. Li (2008). *J. Appl. Phys.* **104**, 124108.
55. I. Sieber, H. Hildebrand, A. Friedrich, and P. Schmuki (2005). *Electro-chem. Commun.* **7**, 97–100.
56. H. Tsuchiya, J. Macak, I. Sieber, and P. Schmuki (2005). *Small* **1**, 722–725.
57. N. K. Allam, X. J. Feng, and C. A. Grimes (2008). *Chem. Mater.* **20**, 6477–6481.
58. H. Tsuchiya, J. M. Macak, I. Sieber, L. Taveira, A. Ghicov, K. Sirotna, and P. Schmuki (2005). *Electrochem. Commun.* **7**, 295–298.